Modelling of Ultrafast Waveguided Electro-Absorption Modulator at Telecommunication Wavelength (λ=1.55 µm) based on Intersubband Transition in an InGaAs/AlAs/AlAsSb Asymmetric Coupled Double Quantum Well Lattice-matched to InP

Pouyan Matin, Jiang Wu, *Senior Member, IEEE*, Huiyun Liu, James Seddon
and Alwyn Seeds, *Life Fellow, IEEE*

Abstract—We investigated theoretically a waveguided EAM (Electro-Absorption Modulator) based on ISBT (Intersubband Transitions) in an $In_{(0.53)}Ga_{(0.47)}As/AlAs/AlAs_{(0.56)}Sb_{(0.44)}$ A-CDQWs (Asymmetric Coupled Double Quantum Wells) lattice-matched to InP at telecommunication wavelength (λ=1.55 µm) which offers ultrahigh-speed and moderate voltage swing. Likewise, the temperature dependency in the $In_{(0.53)}Ga_{(0.47)}As/AlAs/AlAs_{(0.56)}Sb_{(0.44)}$ A-CDQWs was investigated at different temperatures from 300 K to 400 K and evidently the InP-based ISB (Intersubband) modulator offers better temperature stability (~ 0.05 nm/C) compared to the InP-based IB (Interband) modulator. The EAM investigated here is anticipated to have a RC-limited speed (f_{3dB}) of ~ 300 GHz with insertion loss of 5.1 dB, 10 dB extinction ratio and 5.18 dB/V modulation efficiency at a peak-to-peak voltage of 2.0 V which can support a data rate of up to 600 Gbps and beyond.

Index Terms— Asymmetric Coupled Double Quantum Well, Electro-absorption modulator (EAM), InGaAs/AlAs/AlAsSb, intersubband transition, optical waveguide, opto-electronic device.

P. Matin, H. Liu, J. Seddon, and A. Seeds are with the Department of Electronic and Electrical Engineering, University College London, London, WC1E 7JE, U.K. (email: pouyan.matin.17@ucl.ac.uk; huiyun.liu@ucl.ac.uk; james.seddon@ucl.ac.uk; a.seeds@ucl.ac.uk).

J. Wu is with the Institute of Fundamental and Frontier Sciences, University of Electronic Science and Technology of China (UESTC), Chengdu 610054, China. (email: jiangwu@uestc.edu.cn).

I. INTRODUCTION

ULTRAFAST opto-electronic devices such as high-speed photonic switches, high-speed photo-detectors and specifically ultrafast modulators which can function in the fs time scale are increasingly required for achieving high speed data transmission ~ 400 Gb/s per channel for the next generation of information and telecommunication networks [1],[2]. In conventional optical devices including InP-based EAMs which are functioning based on IBT (Interband Transitions) such as Interband-based InP-based EAMs, the carrier relaxation time is limited to the range between a few ps and ns, and also the absorption recovery time is restricted to ~ 5 ps; thus, only a bandwidth of around 80 Gb/s could be achieved [3]-[5]. This restriction of speed is due to the comparatively slow interband recombination lifetimes caused by the limited absorption saturation recovery time which is restricted by the sweep-out time of the photo-generated carriers [6],[7]. Alternatively, by limiting electrons in a Quantum Well (QW) structure and then employing the optical transition among allowable electron energy levels quantized in the well between the subbands of the same generic band such as conduction band and valance band, which is well known as an Inter Sub-Band Transition (ISBT), extremely short absorption recovery time owing to the extremely fast carrier relaxation process can be achieved [8]-[11]. An ultrafast absorption recovery time of 1.3 ps has been reported at 1.3 µm in InP-based $In_{(0.53)}Ga_{(0.47)}As/AlAs/AlAs_{(0.56)}Sb_{(0.44)}$ CDQWs (Coupled Double Quantum Well) structures; though, an ultrafast absorption recovery time of 800 fs could be attained by exploring energy levels higher than the Fermi level in the conduction band [12]. ISBTs in A-CDQWs (Asymmetric-Coupled Double Quantum Well) offer unique properties such as fast relaxation times (sub-fs), large oscillator strengths and

extensive wavelength tuneability [13]-[16]. Likewise, large absorption can be achieved by using ISBTs; therefore, the intersubband modulator is a very promising candidate for the high-speed and low-voltage EAMs of the future [17]. ISBTs-based EAMs offer significant advantages including large bandwidth, low voltage swing, extremely high saturation intensity and negative effective chirp; hence, they are promising candidates for delivering the next generation optical communication systems at 400 Gb/s and beyond [16]-[20]. For attaining ISBTs in the near-infrared region, a large conduction band offset between the well material and the barrier material is essential [21],[22]. InGaAs/AlAsSb as part of wide bandgap antimonides semiconductors owing to its large conduction band offset (~ 1.75 eV), sufficiently large bandgap and low absorption saturation intensity is an appropriate material for realizing near-infrared ISBTs for operation at communications wavelengths between 1.3 μm and 1.55 μm [22],[23]. Moreover, InGaAs/AlAsSb offers ultrafast absorption response time at both 1.3 μm and 1.55 μm, in addition to the capability of being grown by MBE on InP substrate, and also can be monolithically integrated with other optical or electrical components; hence, InGaAs/AlAsSb is a good candidate for ultra-fast InP-based EAMs to be employed in the future optical communication networks [24]-[26].

The purpose of this paper is to report an efficient ultrafast waveguided ISBT-based electro-absorption modulator design based on $In_{(0.53)}Ga_{(0.47)}As/AlAs/AlAs_{(0.56)}Sb_{(0.44)}$ A-CDQWs lattice-matched to InP for delivering the next generation optical communication systems at 400 Gb/s and beyond. The EAM designed here is expected to have a RC-limited speed (f_{3dB}) of 300 GHz with insertion loss of 5.1 dB, 10 dB extinction ratio and 5.18 dB/V modulation efficiency at a peak-to-peak voltage of 2.0 V which can support a data rate of up to 600 Gbps and beyond.

Fig.1 shows schematic of a quantum well structure and some of the different optical transitions possible including IBT (interband transition) and ISBT (intersubband transition).
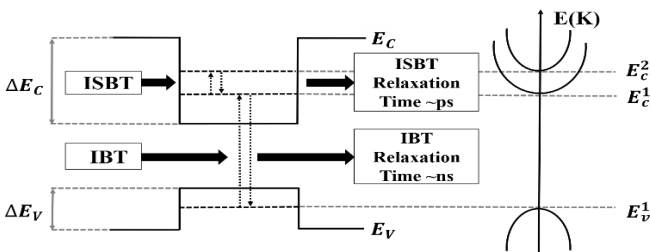

Fig.1. Schematic of a quantum well structure and some of the different optical transitions possible including IBT (interband transition) and ISBT (intersubband transition).

II. MODULATOR DESIGN

We investigate theoretically a modulator design based on ISBTs in InGaAs/AlAsSb A-CDQWs for attaining a useful ISBT (ΔE=0.8 eV) for the telecommunication wavelength (1.55 μm). The DQWs (Double Quantum Well) structure offers much more appropriate absorption in comparison to the SQW (Single Quantum Well) structure for electro-absorption modulation purpose; hence, the DQWs model is advantageous for achieving communication wavelength intersubband gaps between 1.3 μm

and 1.55 μm mostly owing to the achievable sufficient absorption, flexibility in altering quantized energy levels and also carrier relaxation procedures [12],[13]. ISBTs at communication wavelengths can be attained in the DQWs structures by varying the well width, the middle barrier width and also the carrier population in the conduction subband states [12],[23],[27]. Weakly-coupled DQWs structures are more appropriate for electro-absorption modulation compared to the strongly-coupled DQWs structures as in a weakly-coupled DQWs structures the absorption change per volt applied is larger; hence, the absorption edge can be controlled over a larger range of applied electric field as well as equally external voltages [3],[28]. Likewise, the bipolar chirp parameter nearby the central absorption peak is attained in the weakly-coupled DQWs structures which makes it a great potential application in fibre-based optical telecommunication networks [3],[28]. Moreover, A-CDQWs is more advantageous in comparison to the S-CDQWs (Symmetric Coupled Double Quantum Wells); thus, an asymmetric weakly-coupled DQWs is the most appropriate structure to be employed in ultrafast waveguided ISBT-based EAM design. AlAs material must be utilised as a stopping layers and also the central barrier for solving the interface issue in the InGaAs/AlAsSb A-CDQWs structure which is mainly due to the robust intermixing of In, As and Sb in the barrier material and well material [26]-[30]. By employing AlAs, the inter-diffusion related effects at the interface are significantly reduced; consequently, short wavelength ISBTs peak can be attained [29],[30]. Fig.2 shows the conduction band profile and calculated subbands energies of the designed $In_{(0.53)}Ga_{(0.47)}As/AlAs/AlAs_{(0.56)}Sb_{(0.44)}$ A-CDQWs by Nextnano software with no applied bias. The widths of wells and barriers within the A-CDQWs structure were designed for the ISBT between subband 2 and subband 3 (ΔE → E3-E2) to match the 1.55 μm communication wavelength (ΔE ≈ 0.8 eV). We employed 20 periods (20 x 50 nm = 1000 nm) of $In_{(0.53)}Ga_{(0.47)}As/AlAs/AlAs_{(0.56)}Sb_{(0.44)}$ A-CDQWs with outer left barrier ($AlAs_{(0.56)}Sb_{(0.44)}$) width of 10 nm, left stopping layer (AlAs) width of 1 nm, left well ($In_{(0.53)}Ga_{(0.47)}As$) width of 3 nm doped to 1×10^{17} cm^{-3}, inner barrier (AlAs) width of 3 nm, right well ($In_{(0.53)}Ga_{(0.47)}As$) width of 2 nm doped to 1×10^{17} cm^{-3}, right stopping layer (AlAs) width of 1 nm and outer right barrier ($AlAs_{(0.56)}Sb_{(0.44)}$) of 30 nm. The calculated E1-E4 ISBT and E2-E3 ISBT in the proposed $In_{(0.53)}Ga_{(0.47)}As/AlAs/AlAs_{(0.56)}Sb_{(0.44)}$ A-CDQWs are ~ 1.13 eV and ~ 0.8 eV, respectively. The calculated ISBTs are very close to the achieved ISBTs by Ishikawa *et al.* [30].
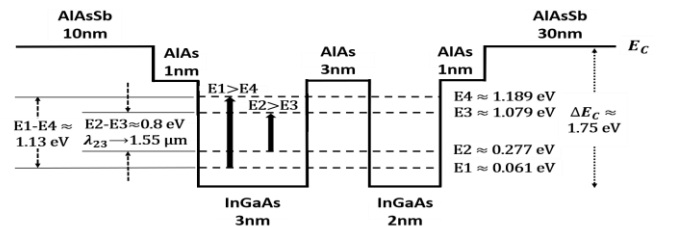

Fig.2. Conduction band profile and calculated subbands energies of the designed $In_{(0.53)}Ga_{(0.47)}As/AlAs/AlAs_{(0.56)}Sb_{(0.44)}$ A-CDQWs with no applied bias. Materials and thickness used for different layers are specified along with the calculated energy levels.

Fig.3 shows the layer structure for the $In_{(0.53)}Ga_{(0.47)}As/AlAs/AlAs_{(0.56)}Sb_{(0.44)}$ A-CDQWs employed for the ISBT-based EAM.
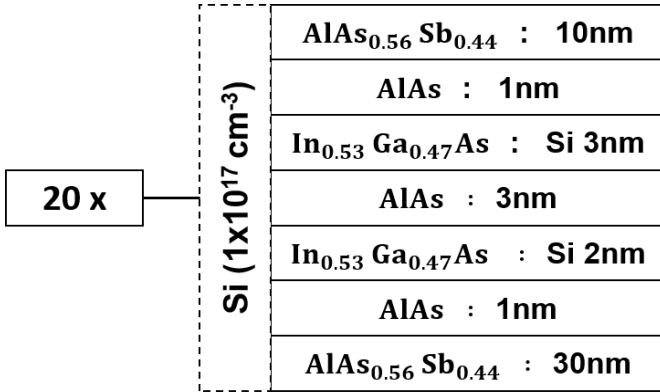
Fig.3. The layer structure for the $In_{(0.53)}Ga_{(0.47)}As/AlAs/AlAs_{(0.56)}Sb_{(0.44)}$ A-CDQWs employed for the ISBT-based EAM.

III. ISB TEMPERATURE DEPENDENCY

When the temperature is increased from 300 K to 400 K in the $In_{(0.53)}Ga_{(0.47)}As/AlAs/AlAs_{(0.56)}Sb_{(0.44)}$ A-CDQWs lattice-matched to InP, the associated subband energies (E1, E2, E3 and E4), the E1-E4 ISBT and also the E2-E3 ISBT are decreased significantly. Additionally, the E2-E3 ISBT is decreased less in comparison to the E1-E4 ISBT which means the E2-E3 ISBT offers better temperature stability in comparison to the E1-E4 ISBT in the $In_{(0.53)}Ga_{(0.47)}As/AlAs/AlAs_{(0.56)}Sb_{(0.44)}$ A-CDQWs lattice-matched to InP. Moreover, the rate of change of wavelength associated to E2-E3 ISBT is smaller than the rate of change of wavelength associated to E1-E4 ISBT in the $In_{(0.53)}Ga_{(0.47)}As/AlAs/AlAs_{(0.56)}Sb_{(0.44)}$ A-CDQWs lattice-matched to InP; therefore, principally owing to the offered better temperature stability by E2-E3 ISBT in comparison to the E1-E4 ISBT, the E2-E3 ISBT is the more suitable ISBT to be chosen for designing an ISBT-based EAM. Furthermore, The rate of change of wavelength based on temperature in InP-based interband modulator is ~ 0.5 nm/C [31]; however, the rate of change of wavelength offered by ISBTs in the $In_{(0.53)}Ga_{(0.47)}As/AlAs/AlAs_{(0.56)}Sb_{(0.44)}$ A-CDQWs lattice-matched to InP is almost 10 times better (~ 0.05 nm/C) which means that InP-based ISB modulator offers much better temperature stability compared to the InP-based IB modulator. Fig.4. shows subband energies (E1, E2, E3 and E4) of the $In_{(0.53)}Ga_{(0.47)}As/AlAs/AlAs_{(0.56)}Sb_{(0.44)}$ A-CDQWs with outer left barrier ($AlAs_{(0.56)}Sb_{(0.44)}$) width of 10 nm, left stopping layer (AlAs) width of 1 nm, left well ($In_{(0.53)}Ga_{(0.47)}As$) width of 3 nm doped to $1x10^{17}\,cm^{-3}$, inner barrier (AlAs) width of 3 nm, right well ($In_{(0.53)}Ga_{(0.47)}As$) width of 2 nm doped to $1x10^{17}\,cm^{-3}$, right stopping layer (AlAs) width of 1 nm and outer right barrier ($AlAs_{(0.56)}Sb_{(0.44)}$) of 30 nm lattice-matched to InP (a) and two relevant ISBTs including E1-E4 (b) and E2-E3 (c) under different temperatures from 300 K to 400 K, and also the inset shows the wavelength associated to E1-E4 ISBT (b) and the wavelength associated to E2-E3(c).

Fig.4. Subband energies (E1, E2, E3 and E4) of the $In_{(0.53)}Ga_{(0.47)}As/AlAs/AlAs_{(0.56)}Sb_{(0.44)}$ A-CDQWs lattice-matched to InP (a) and two relevant ISBTs including E1-E4 (b) and E2-E3 (c) under different temperatures from 300 K to 400 K. The inset shows the wavelength associated to E1-E4 ISBT (a) and the wavelength associated to E2-E3(b).
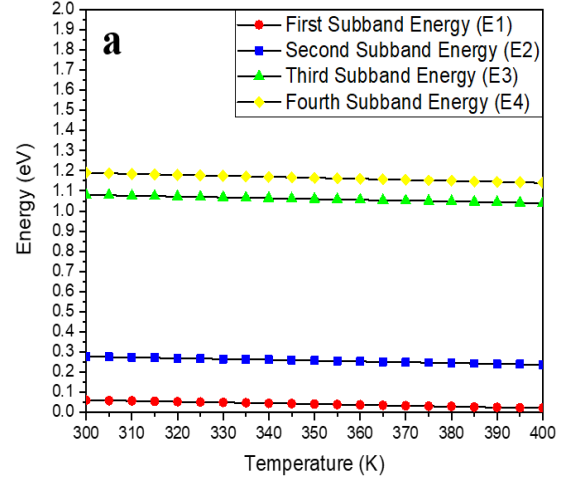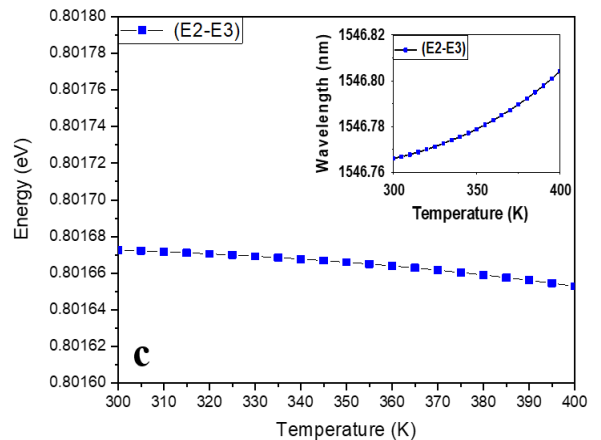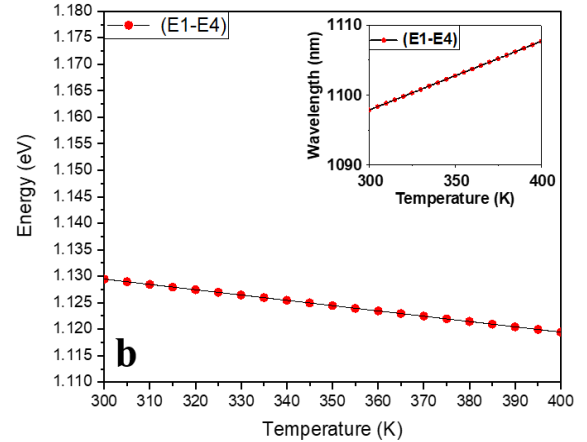
IV. WAVEGUIDE DESIGN AND CONTACTING

For designing an ultrafast ISBT-based EAM, employment of an optical waveguide with lower loss is essential; therefore, a newly designed ISBT-based waveguide device is employed. For this purpose, the active region ($In_{0.53}Ga_{0.47}As/AlAs/AlAs_{0.56}Sb_{0.44}$ A-CDQWs) as core layer is sandwiched with InAlAs as top and bottom cladding layers. The InAlAs is selected mainly due to the match interface with the active region; however, the refractive index of the InAlAs (~ 3.23) is still an issue as it is higher than the average refractive index of the $In_{0.53}Ga_{0.47}As/AlAs/AlAs_{0.56}Sb_{0.44}$ A-CDQWs (~ 3.13); thus, 70 nm high refractive index InGaAlAs (~ 3.46) doped to 2×10^{17} cm^{-3} guiding layers on both sides of the A-CDQWs are employed in addition to the 1.43 nm InAlAs doped to 2×10^{18} cm^{-3} for confining the optical mode in the core region. Moreover, 300 nm $In_{0.53}Ga_{0.47}As$ doped to 2×10^{19} cm^{-3} is employed as top contact (Schottky contact) and 500 nm $In_{0.53}Ga_{0.47}AsP$ doped to 3×10^{18} cm^{-3} is employed as bottom contact (Ohmic contact). Fig.5. shows the ISBT-based $In_{0.53}Ga_{0.47}As/AlAs/AlAs_{0.56}Sb_{0.44}$ A-CDQWs waveguide device.

Fig.6. The ISBT-based $In_{0.53}Ga_{0.47}As/AlAs/AlAs_{0.56}Sb_{0.44}$ A-CDQWs waveguide mode profile.
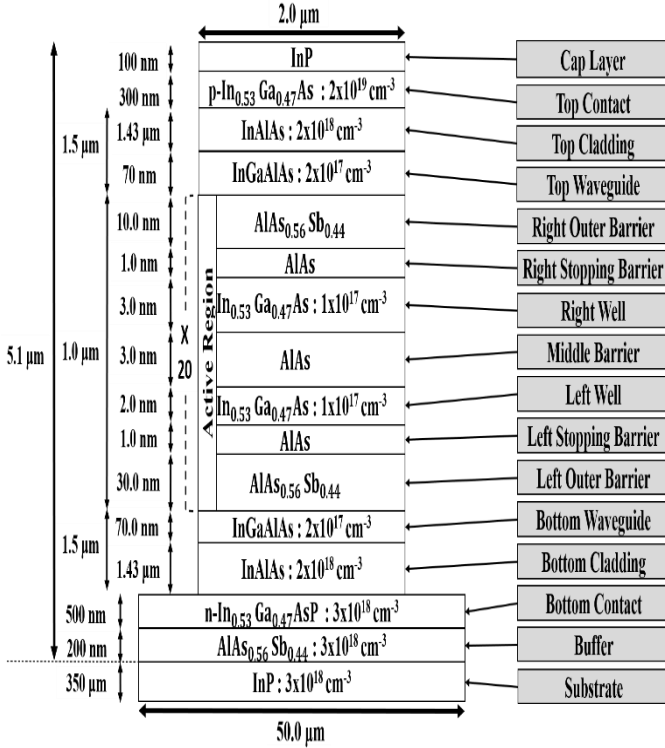
Fig.5. The ISBT-based $In_{0.53}Ga_{0.47}As/AlAs/AlAs_{0.56}Sb_{0.44}$ A-CDQWs waveguide device. The refractive index (n) of InP, AlAs, InGaAs, InAlAs, InGaAlAs, InGaAsP, $AlAs_{0.56}Sb_{0.44}$, $In_{0.53}Ga_{0.47}As$ and $In_{(0.53)}Ga_{(0.47)}As/AlAs/AlAs_{(0.56)}Sb_{(0.44)}$ A-CDQWs are 3.17, 2.95, 3.57, 3.23, 3.46, 3.39, 3.12, 3.59 and 3.13, respectively. Additionally, the absorption coefficients (α) of E1-E4 ISBT in $In_{(0.53)}Ga_{(0.47)}As/AlAs/AlAs_{(0.56)}Sb_{(0.44)}$ A-CDQWs, E2-E3 ISBT in $In_{(0.53)}Ga_{(0.47)}As/AlAs/AlAs_{(0.56)}Sb_{(0.44)}$ A-CDQWs, InGaAs, InGaAlAs and InAlAs are $832\ cm^{-1}$, $2548\ cm^{-1}$, $5500\ cm^{-1}$, $5000\ cm^{-1}$, $4500\ cm^{-1}$, respectively.

Fig.6. shows the ISBT-based $In_{0.53}Ga_{0.47}As/AlAs/AlAs_{0.56}Sb_{0.44}$ A-CDQWs waveguide mode profile.
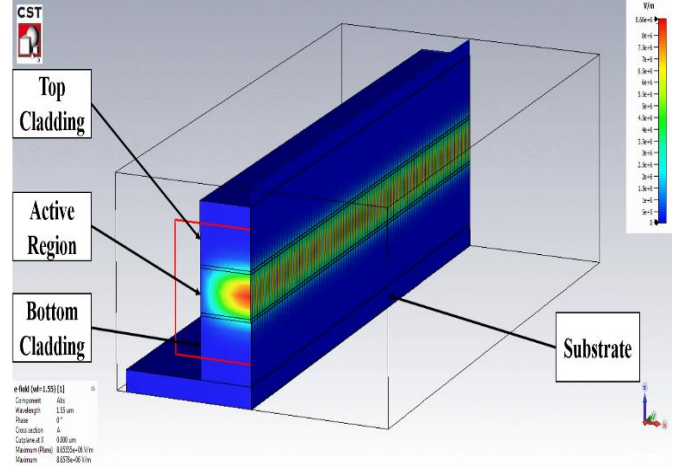
V. INTERSUBBAND ABSORPTION COEFICIENT CALCULATION

ISBA (Intersubband Absorption) occurs owing to the interaction of an electromagnetic field with the electronic transitions among the confined states in quantum wells in the conduction band or in the valance band [32],[33]. Owing to an intrinsic insensitivity to saturation due to the extremely fast carrier relaxation time, large absorption could be achieved by ISBTs [33]. ISBA coefficient is determined by [33]

$$\alpha(\hbar\omega) = \frac{\omega\mu c e^2 m^* K_b T}{\pi \hbar^2 L n_r} \sum_{i<f} In\left\{ \frac{1 + \exp\left[(E_F - E_i)/K_b T\right]}{1 + \exp\left[(E_F - E_f)/K_b T\right]} \right\} \quad (1)$$

$$\times <z>^2 \frac{(\Gamma/2)}{(E_{if} - \hbar\omega)^2 + (\Gamma/2)^2}$$

Where, $<z> = <Q_f.|z|.Q_i> = \int Q_f.z.Q_i\ dz$

Where, ω is the angular frequency, μ is the permeability of the A-CDQWs , C is the speed of light, e is the charge of an electron, K_b is the Boltzmann constant, T is the temperature in Kelvin, Γ is the line width or full-width at half-maximum (FWHM), E_i is the initial subband energy (E1 or E2), E_f is the final subband energy (E3 or E4), $\emptyset_i$ is the envelope function of the initial subband (E1 or E2) and finally $\emptyset_f$ is the envelope function of the final subband (E3 or E4).

Likewise, m^* is the weighted effective mass which is calculated by [33]

$$m^* = \left(m_w^* L_w + m_w^* L_b\right)/\left(L_w + L_b\right) \quad (2)$$

Furthermore, n_r is the refractive index of the A-CDQWs which is calculated by [33]

$$n_r = \left(n_w \ L_w + n_b \ L_b \right)/\left(L_w + L_b \right) \tag{3}$$

Where, L_w is the well width, L_b is the middle barrier width, n_w is the well refractive index and n_b is the barrier refractive index in the A-CDQWs.

1.55 μm ISBA in $In_{(0.53)}Ga_{(0.47)}As/AlAs_{(0.56)}Sb_{(0.44)}$ A-CDQWs was first reported by Mozume *et al.* [11]. The calculated ISBA coefficients (α) of the $In_{(0.53)}Ga_{(0.47)}As/AlAs/AlAs_{(0.56)}Sb_{(0.44)}$ A-CDQWs structure is 832 cm^{-1} for E1-E4 ISBT and 2548 cm^{-1} for E2-E3 ISBT. The evaluated ISBA coefficients (α) of the $In_{(0.53)}Ga_{(0.47)}As/AlAs/AlAs_{(0.56)}Sb_{(0.44)}$ A-CDQWs are close to the achieved ISBA coefficients by Yoshida *et al.* [20] and Neogi *et al.* [23]. By employment of the optical waveguide structure, the ISBA coefficient of the both E1-E4 ISBT and also E2-E3 ISBT are reduced significantly. The waveguide absorption coefficient is calculated by [32]

$$\alpha_{WG} = \alpha_{Core} \times \Gamma_{Core} \tag{4}$$

Where, α_{Core} is the ISBA coefficient (α) of the core layer ($In_{(0.53)}Ga_{(0.47)}As/AlAs/AlAs_{(0.56)}Sb_{(0.44)}$ A-CDQWs) of the waveguide structure and Γ_{Core} refers to the confinement factor of the core layer which defines the overlap of the optical mode with the core layer of the waveguide. The waveguide ISBA coefficient (α_{WG}) for the E1-E4 ISBT and also the E2-E3 ISBT are calculated by [32]

$$\alpha_{WG(E_1-E_4)} = \alpha_{Core(E_1-E_4)} \times \Gamma_{Core}$$
$$\& \tag{5}$$
$$\alpha_{WG(E_2-E_3)} = \alpha_{Core(E_2-E_3)} \times \Gamma_{Core}$$

The core confinement factor (Γ_{Core}) is described as a ratio of the mode intensity $E^2(x)$ overlapping with the core layer to the entire mode intensity $E^2(x)$ in the whole waveguide structure which is determined by [32]

$$\Gamma_{Core} = \frac{\int_{-d/2}^{+d/2} E^2 \left(x \right) dx}{\int_{-\infty}^{+\infty} E^2 \left(x \right) dx} \tag{6}$$

Where, *d* refers to the thickness of the core layer and *E* refers to the mode intensity. The mode was simulated using FDTD. The calculated mode intensity overlapping with the core layer is $\sim 3.45 \times 10^{-10}$ and the total mode intensity in the whole waveguide is $\sim 4.15 \times 10^{-10}$; consequently, the calculated core confinement factor (Γ_{Core}) for the $In_{(0.53)}Ga_{(0.47)}As/AlAs/AlAs_{(0.56)}Sb_{(0.44)}$ A-CDQWs waveguide structure is $\sim 85\%$. Furthermore, the waveguide ISBA coefficient (α_{WG}) of the $In_{(0.53)}Ga_{(0.47)}As/AlAs/AlAs_{(0.56)}Sb_{(0.44)}$ A-CDQWs waveguide structure is 707 cm^{-1} for E1-E4 ISBT and 2167 cm^{-1} for E2-E3 ISBT; though, the ISBA coefficient of the E1-E4 ISBT and E2-E3 ISBT within the well region ($In_{(0.53)}Ga_{(0.47)}As$) of the $In_{(0.53)}Ga_{(0.47)}As/AlAs/$

$AlAs_{(0.56)}Sb_{(0.44)}$ A-CDQWs waveguide structure are much lower as only small part of the optical mode within the waveguide structure overlaps with the available wells within the core layer (active region). The well ISBA coefficient is calculated by [32]

$$\alpha_{Well} = \alpha_{WG} \times \Gamma_{Well} \tag{7}$$

Where, α_{WG} is the waveguide ISBA coefficient of the waveguide structure and Γ_{Well} refers to the well confinement factor which defines the overlap of the optical mode with the wells in the $In_{(0.53)}Ga_{(0.47)}As/AlAs/AlAs_{(0.56)}Sb_{(0.44)}$ A-CDQWs . The well ISBA coefficient for the E1-E4 ISBT and the E2-E3 ISBT are calculated by [32]

$$\alpha_{Well(E_1-E_4)} = \alpha_{WG(E_1-E_4)} \times \Gamma_{Well}$$
$$\& \tag{8}$$
$$\alpha_{Well(E_2-E_3)} = \alpha_{WG(E_2-E_3)} \times \Gamma_{Well}$$

The confinement factor (Γ_{Well}) is described as a ratio of the mode intensity $E^2(x)$ overlapping with the wells to the entire mode intensity $E^2(x)$ in the whole active region which is determined by [32]

$$\Gamma_{Well} = \frac{\int_{-d/2}^{+d/2} E^2 \left(x \right) dx}{\int_{-\infty}^{+\infty} E^2 \left(x \right) dx} \tag{9}$$

Where, *d* refers to the thickness of the well and *E* refers to the mode intensity. The mode was simulated using FDTD. The calculated mode intensity overlapping with the well is $\sim 2.43 \times 10^{-10}$ and the total mode intensity in the whole waveguide is $\sim 4.15 \times 10^{-10}$; thus, the calculated well confinement factor (Γ_{Well}) for the $In_{(0.53)}Ga_{(0.47)}As/AlAs/AlAs_{(0.56)}Sb_{(0.44)}$ A-CDQWs waveguide structure is $\sim 10\%$. The calculated ISBA coefficient in the waveguided ISBT-based $In_{(0.53)}Ga_{(0.47)}As/AlAs/AlAs_{(0.56)}Sb_{(0.44)}$ A-CDQWs for E1-E4 ISBT and for E2-E3 ISBT is 71 cm^{-1} and 217 cm^{-1}, respectively.

VI. RESULTS AND DESCUSSION

The electro-absorption modulator length is determined by [34]

$$L = \frac{1}{\alpha_{(E_2-E_3)}} \tag{10}$$

Where, L is the EAM length and $\alpha_{(E2-E3)}$ is the ISBA coefficient for the E2-E3 ISBT in the $In_{(0.53)}Ga_{(0.47)}As/AlAs/AlAs_{(0.56)}Sb_{(0.44)}$ A-CDQWs waveguided structure under no electric field which is 217 cm^{-1}. The calculated EAM length is ~ 46 μm. Moreover, the calculated V_{bd} (breakdown voltage) is

~ 10 V. External electric field has a large influence on the subband energies as well as equivalent wavefunctions which can control the variation of ISBA [33]. ISB-based EAMs operate based on the variation of the absorption spectrum which is caused by an applied electric field [33]. Fig.7. shows the ISBA coefficients for E2-E3 ISBT in the $In_{(0.53)}Ga_{(0.47)}As/$ $AlAs/AlAs_{(0.56)}Sb_{(0.44)}$ A-CDQWs waveguided structure (a), the related extinction ratio (b) and the related modulation efficiency (c) under different applied electric field from 0 kV/cm to 60 kV/cm (reverse bias from 0 V to -6 V) where the EAM length is 46 μm.

Fig.7. The ISBA coefficients for E2-E3 ISBT in the $In_{(0.53)}Ga_{(0.47)}As/$ $AlAs_{(0.56)}Sb_{(0.44)}$ A-CDQWs waveguided structure (a), the related extinction ratio (b) and the related modulation efficiency (c) under different applied electric field from 0 kV/cm to 60 kV/cm (reverse bias from 0 V to -6 V) where the EAM length is 46 μm.
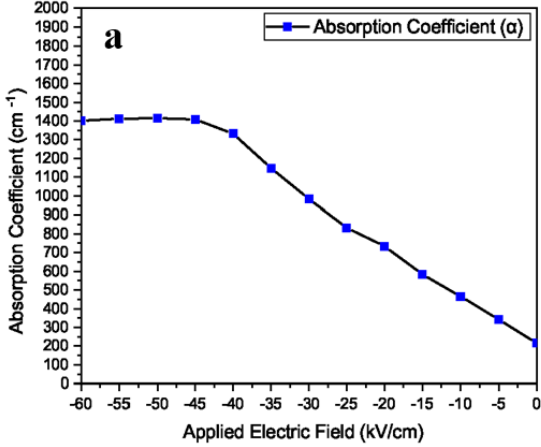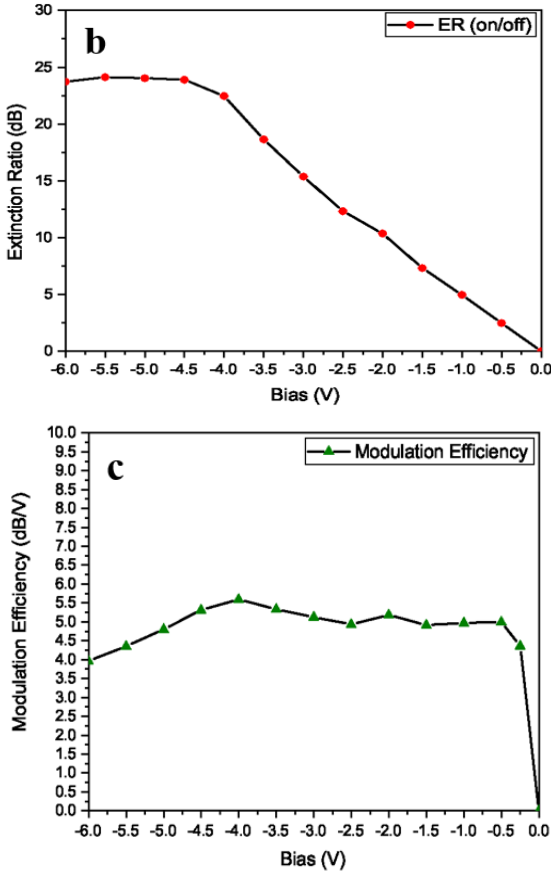

The ISBA coefficient for E2-E3 ISBT increases when the applied negative electric field (reverse bias) increases from 0 kV/cm to 50 kV/cm (0 V to -5 V); however, when the applied electric field increases from 50 kV/cm to 60 kV/cm (-5 V to -6 V), the ISBA coefficient for E2-E3 ISBT is decreased slightly which is due to the absorption saturation. The ER (extinction ratio) is calculated by [34]

$$R_{on/off} = \frac{P_{out}\left(V_{on} = 0\right)}{P_{out}\left(V_{off} = V\right)} = \frac{e^{-\alpha(0)L}}{e^{-\alpha(V)L}} \quad (11)$$

Where, $\alpha(0)$ is the ISBA coefficients for E2-E3 ISBT ($\alpha_{ISB(E2-E3)}$) at 0 V, $\alpha(V)$ is the ISB absorption coefficients for E2-E3 ISBT with applied reverse bias and L is the EAM length. Moreover, the ER (extinction ratio) in dB (decibel) is calculated by [34]

$$R_{on/off}\left(dB\right) = 10\log\left(R_{on/off}\right) = 4.343\left[\alpha(V) - \alpha(0)\right]L \quad (12)$$

The extinction ratio increases when the reverse bias increases from 0 V to -5.5 V; however, when -6 V reverse bias is applied, the ER is decreased slightly which is obviously owing to the absorption saturation.

The modulation efficiency is calculated by [34]

$$\frac{R_{on/off}}{\Delta V} = 4.343 \frac{\left[\alpha(V) - \alpha(0)\right]L}{\Delta V} = 4.343 \frac{\Delta\alpha}{\Delta F} \quad (13)$$

Where, $\alpha(0)$ is the ISBA coefficient for E2-E3 ISBT ($\alpha_{ISB(E2-E3)}$) at 0 V, $\alpha(V)$ is the ISBA coefficient for E2-E3 ISBT with applied reverse bias and L is the EAM length. Likewise, $\Delta\alpha$ is the ISBA coefficient difference, ΔV is the applied reverse bias difference and ΔF is the applied negative electric field difference. The modulation efficiency increases largely when the reverse bias increases from 0 V to -0.5 V. Moreover, the modulation efficiency is almost the same from -0.5 V up to -4.0 V which is ~ 5.0 dB/V; though, the modulation efficiency is decreased from -4.0 V to -6.0 V.

Fig.8. shows the extinction ratio under different reverse bias from 0 V to -2 V (0 kV/cm to 20 kV/cm) for different EAM lengths including 46 μm, 60 μm, 70 μm, 80 μm, 90 μm and 100 μm (a), and the insertion loss in different EAM lengths including 46 μm, 60 μm, 70 μm, 80 μm, 90 μm and 100 μm (b). In different EAM lengths, when the applied reverse bias is increased from 0 V to -2 V (0 kV/cm to 20 kV/cm), the extinction ratio is also increased. Moreover, when the length of the EAM is increased, the extinction ratio is largely increased. Furthermore, the rate of change of the extinction ratio is linear with length and voltage.
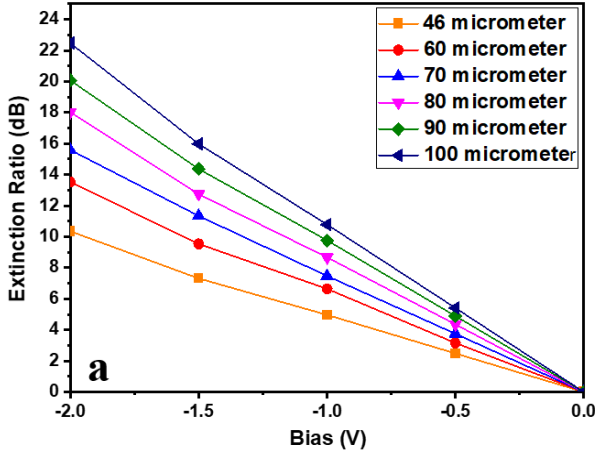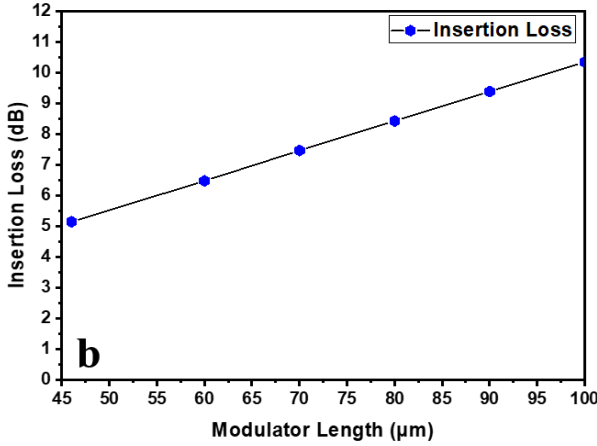
Fig.8. The extinction ratio under different reverse bias from 0 V to -2 V (0 kV/cm to 20 kV/cm) for different EAM lengths including 46 μm, 60 μm, 70 μm, 80 μm, 90 μm and 100 μm (a), and the insertion loss in different EAM lengths including 46 μm, 60 μm, 70 μm, 80 μm, 90 μm and 100 μm (b).

The IL (insertion loss) in the $In_{(0.53)}Ga_{(0.47)}As/AlAs/AlAs_{(0.56)}Sb_{(0.44)}$ A-CDQW is calculated by [34]

$$IL = \frac{P_{in}}{P_{out}(V=0)} = e^{-\alpha(0)L} \tag{14}$$

Where, $\alpha(0)$ is the ISBA coefficient for E2-E3 ISBT ($\alpha_{ISB(E2-E3)}$) at 0 V and L is the EAM length. Moreover, the IL (insertion loss) in dB (decibel) is calculated by [34]

$$IL(dB) = 10\log\left(e^{-\alpha(0)L}\right) \tag{15}$$

The calculated insertion loss of the waveguided EAM with length of 46 μm is ~ 5.1 dB. It must be mentioned that the calculated insertion loss includes the loss in the $In_{(0.53)}Ga_{(0.47)}As/AlAs/AlAs_{(0.56)}Sb_{(0.44)}$ A-CDQW (active region) and other layers of the waveguided EAM structure which are overlapped with the optical mode; however, it does not include the coupling loss into and out of the EAM. When the length of the EAM is increased, the insertion loss is increased significantly; therefore, the EAM length has direct relationship with the insertion loss.

By reducing the length of the EAM, a very low insertion loss of ≤ 1 dB could be achieved which results in larger optical bandwidth (f_{3dB}) as well as higher data rate; however, the extinction ratio and also the modulation efficiency will be decreased significantly.

Fig.9. shows electrical equivalent circuit of the waveguided ISBT-based $In_{(0.53)}Ga_{(0.47)}As/AlAs/AlAs_{(0.56)}Sb_{(0.44)}$ A-CDQWs EAM, where V_{in} is the bias voltage, L is the inductance, C_p is the parasitic capacitance, C_d is the device capacitance, R_{in} is the line resistance, R_{acc} is the access resistance and R_d is the device resistance.

Fig.9. Electrical equivalent circuit of the waveguided $In_{(0.53)}Ga_{(0.47)}As/AlAs/AlAs_{(0.56)}Sb_{(0.44)}$ A-CDQWs EAM where V_{in} is the bias voltage, L is the inductance, C_p is the parasitic capacitance, C_d is the device capacitance, R_{in} is the line resistance, R_{acc} is the access resistance and R_d is the device resistance.
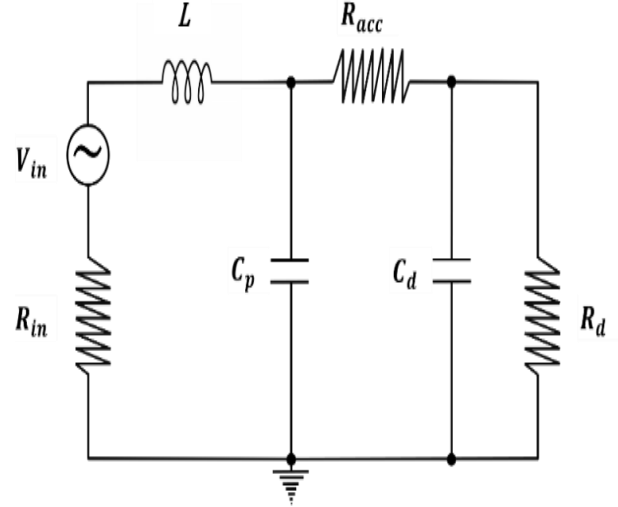
In case of EAM, the p-i-n structure can be estimated by a first-order RC low-pass filter, which is considered by an operative capacitor (C) and the active resistance (R); therefore, the 3dB bandwidth (f_{3dB}) is determined by the RC constant. The 3dB bandwidth (f_{3dB}) is calculated by [34]

$$f_{3dB} = \frac{1}{2\pi RC} \tag{16}$$

Where, C is the device capacitance (C_d) and R is the active resistance which is the combination of the access resistance (R_{acc}) and the line resistance (R_{in}). For calculating the optical bandwidth (f_{3dB}), the device resistance (R_d) has been ignored as the device is operated by reverse bias (0 V → -2.0 V). Moreover, the inductance (L) is related to the packaging which has been ignored. Likewise, the parasitic capacitance (C_p) from the device bond pad has been ignored in this calculation, as it could be minimised by careful design. The device capacitance (C_d) is calculated by [34]

$$C_d = \varepsilon_o \varepsilon_r \frac{WL}{d} \tag{17}$$

Where, ε_o is the vacuum permittivity, ε_r is the dielectric constant of the $In_{(0.53)}Ga_{(0.47)}As/AlAs/AlAs_{(0.56)}Sb_{(0.44)}$ A-CDQWs (11.065), W is the waveguide width (2.0 μm), L is the modulator length (46 μm), and d is the thickness of the $In_{(0.53)}Ga_{(0.47)}As/AlAs/AlAs_{(0.56)}Sb_{(0.44)}$ A-CDQWs (1000 nm). The calculated device capacitance (C_d) is ~ 9 fF which is extremely small and advantageous. As it was mentioned earlier, R which refers to the active resistance is the combination of the access resistance (R_{acc}) and the line resistance (R_{in}). The line resistance (R_{in}) is estimated to be ~ 50 Ω and the access resistance (R_{acc}) is calculated by [32]-[35]

$$R_{acc} = \frac{\rho L}{W_{Lp}} + \frac{\rho L}{W_{Ln}} \tag{18}$$

Where, L is the EAM length, W_{Lp} is the p-contact width, W_{Ln} is the n-contact width and ρ is the electrical resistivity which is the inverse of electrical conductivity and is calculated by [34]

$$\rho = \frac{1}{\delta} \tag{19}$$

Where, δ is the electrical conductivity and is calculated by [34],[35]

$$\delta = eN_d \tag{20}$$

Where, e is the electron charge and N_d is the doping density. The calculated access resistance (R_{acc}) for the p-contact layer (~ 7.19 Ω) and the n-contact layer (~ 1.92 Ω) is ~ 9.11 Ω. As the R_{acc} ($\simeq$ 9.11 Ω) and R_{in} ($\simeq$ 50 Ω) are in series in the electrical equivalent circuit of the waveguided ISBT-based $In_{(0.53)}Ga_{(0.47)}As/AlAs/AlAs_{(0.56)}Sb_{(0.44)}$ A-CDQWs EAM; therefore, the R_Total (R_acc + R_in) is ~ 59.11 Ω which is very small and advantageous. By utilising the calculated active resistance (R_acc + R_in) and active capacitor (C_d), the optical bandwidth (f_{3dB}) is calculated to be ~ 300 GHz which is extremely large and advantageous. By employment of the On-Off keying as the simplest method of ASK (Amplitude-Shift Keying) modulation, an extremely fast data rate of ~ 600 Gbps can be achieved; however, by employing more advanced modulation schemes such as QAM (Quadrature Amplitude Modulation), higher data rate ($\geq$ 1 Tbps) could be attained. It must be noted that the extremely high calculated bandwidth of ~300 GHz is principally the outcome of the employed very narrow waveguide width (2μm), very small device capacitance ($C_d \simeq$ 9 fF) and small access resistance ($R_{acc} \simeq$ 9.11 Ω); however, in practice, by considering all practical factors, the attainable actual electrical bandwidth is $\geq$ 100 GHz which is highly beneficial. Fig.10. shows the rate of change of the RC-limited frequency response (f_{3dB}) in a 50 Ω system for different EAM lengths including 46 μm, 60 μm, 70 μm, 80 μm, 90 μm and 100 μm.
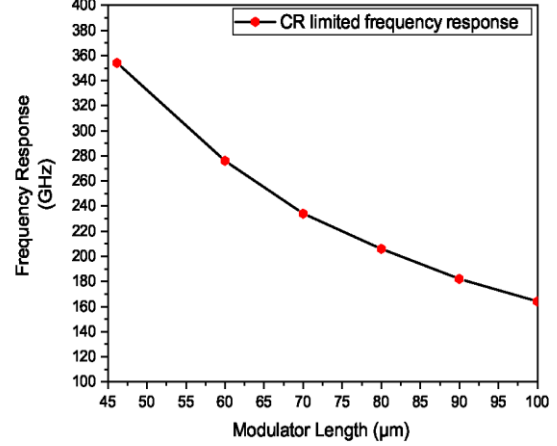

Fig.10. The rate of change of the RC-limited frequency response (f_{3dB}) in a 50 Ω system for different electro-absorption modulator lengths including 46 μm, 60 μm, 70 μm, 80 μm, 90 μm and 100 μm.

The EAM length has direct relationship with the device capacitance (C_d); therefore, when the length of the EAM is increased, the device capacitance (C_d) is also increased. Moreover, when the device capacitance (C_d) is increased, the RC-limited frequency response (f_{3dB}) is decreased largely. In the 50 Ω system, when the length of EAM is ~ 46 μm, the achieved f_{3dB} bandwidth is ~ 354 GHz; however, when the length of the EAM is increased to 100 μm, the achieved f_{3dB} bandwidth is decrease to ~ 164 GHz; thus, when the length of the EAM is increased, the RC-limited frequency response (f_{3dB}) as well as data rate are decreased significantly.

Table 1 represents the comparison between LiNbO_3 MZI (Mach-Zehnder interferometer modulator), IB-based InP EAM and the proposed ISB-based InP EAM based on ISBT in an $In_{(0.53)}Ga_{(0.47)}As/AlAs/AlAs_{(0.56)}Sb_{(0.44)}$ A-CDQWs.

TABLE I
Comparison between LiNbO_3 MZI, IB-based InP EAM and the proposed ISB-based InP EAM based on ISBT in an $In_{(0.53)}Ga_{(0.47)}As/AlAs/AlAs_{(0.56)}Sb_{(0.44)}$ A-CDQWs [36].

	LiNbO_3 MZI	IB-based InP EAM	ISB-based InP EAM
Size	Large (several centimetres)	Small (<500 μm)	Small (<500 μm)
Drive voltage	Medium to low (>5V)	Low (<3V)	Low (<2V)
Bandwidth	Very high (~100 GHz)	Very high (~80 GHz)	Very High (~300 GHz)*
Extinction Ratio	>20dB	>20dB	≥10dB
Insertion loss	Low	Moderate	Moderate (~5.1 dB)

*The anticipated actual electrical bandwidth is ≥ 100 GHz.

The investigated ISB-based InP EAM based on ISBT in $In_{(0.53)}Ga_{(0.47)}As/AlAs/AlAs_{(0.56)}Sb_{(0.44)}$ A-CDQWs with an operating wavelength of 1.55 μm in this paper, is smaller than the LiNbO$_3$ MZI. Moreover, it offers larger bandwidth and requires lower drive voltage in comparison to the LiNbO$_3$ MZI and IB-based InP EAM; however, the proposed ISB-based InP EAM offers lower extinction ratio and larger insertion loss.

VII. CONCLUSION

In conclusion, we have investigated theoretically a waveguided EAM using ISBT in $In_{(0.53)}Ga_{(0.47)}As/AlAs/AlAs_{(0.56)}Sb_{(0.44)}$ A-CDQWs lattice-matched to InP with an operating wavelength of 1.55 μm which offers ultrahigh speed and moderate voltage swing. The desired ISBT (~ 0.8 eV) at 1.55 μm can be achieved in an $In_{(0.53)}Ga_{(0.47)}As/AlAs/AlAs_{(0.56)}Sb_{(0.44)}$ A-CDQWs with outer left barrier ($AlAs_{(0.56)}Sb_{(0.44)}$) width of 10 nm, left stopping layer (AlAs) width of 1 nm, left well ($In_{(0.53)}Ga_{(0.47)}As$) width of 3 nm doped to $1x10^{17}$ cm^{-3}, inner barrier (AlAs) width of 3 nm, right well ($In_{(0.53)}Ga_{(0.47)}As$) width of 2 nm doped to $1x10^{17}$ cm^{-3}, right stopping layer (AlAs) width of 1 nm and outer right barrier ($AlAs_{(0.56)}Sb_{(0.44)}$) of 30 nm. Likewise, the beneficial optical waveguide structure by employing 1.43 nm InAlAs doped to $2x10^{18}$ cm^{-3} and 70 nm InGaAlAs $2x10^{18}$ cm^{-3} as both top and bottom cladding layers and 1000 nm (20 period of 50 nm) $In_{(0.53)}Ga_{(0.47)}As/AlAs/AlAs_{(0.56)}Sb_{(0.44)}$ A-CDQWs (active region) as core region was investigated and designed. Also, the temperature dependency in the proposed $In_{(0.53)}Ga_{(0.47)}As/AlAs/AlAs_{(0.56)}Sb_{(0.44)}$ A-CDQWs lattice-matched to InP was investigated at various temperatures from 300 K to 400 K and evidently the InP-based ISB modulator offers much better temperature stability (~ 0.05 nm/C) compared to the InP-based IB modulator. Likewise, E2-E3 ISBT in the $In_{(0.53)}Ga_{(0.47)}As/AlAs/AlAs_{(0.56)}Sb_{(0.44)}$ A-CDQWs is more advantageous transition in comparison to the E1-E4 ISBT principally due to the offered better temperature stability. Furthermore, rapid changes in ISBA coefficient in the $In_{(0.53)}Ga_{(0.47)}As/AlAs/AlAs_{(0.56)}Sb_{(0.44)}$ A-CDQWs with applied reverse bias (0 V → 2 V) were achieved. The EAM investigated and analysed here is predicted to have a RC-limited speed (f_{3dB}) of ~ 300 GHz with insertion loss of 5.1 dB, 10 dB extinction ratio and 5.18 dB/V modulation efficiency at a peak-to-peak voltage of 2.0 V which can support a data rate of up to ~ 600 Gbps and beyond. It must be pointed out that by reducing the EAM length, a very low insertion loss of ≤ 1 dB could be attained which results in larger optical bandwidth (f_{3dB}) as well as higher data rate. Moreover, by employing more advanced modulation schemes such as QAM, higher data rate (≥ 1 Tbps) could be achieved.

REFERENCES

[1] M. Romagnoli *et al.*, "Graphene-based integrated photonics for next-generation datacom and telecom," *Nat. Rev. Mater.*, vol. 3, no. 10, pp. 392–414, 2018.

[2] M. Beeler, E. Trichas, and E. Monroy, "III-nitride semiconductors for intersubband optoelectronics: A review," *Semicond. Sci. Technol.*, vol. 28, no. 7, 2013.

[3] K. M. Wong and D. W. E. Allsopp, "Intersubband absorption modulation in coupled double quantum wells by external bias," *Semicond. Sci. Technol.*, vol. 24, no. 4, 2009.

[4] O. Wada, "Femtosecond all-optical devices for ultrafast communication and signal processing," *New J. Phys.*, vol. 6, pp. 1–35, 2004.

[5] S. Tsujino, C. Metzner, T. Noda and H. Sakaki, "Saturation of intersubband absorption by real-space transfer in modulation doped single GaAs-AlAs quantum well," *Phys. Stat. Sol. (B)*, Vol. 204, pp. 162-165, 1997.

[6] N. El Dahdah, G Aubin, J.C. Harmand, A. Ramdane, A. Shen, E Devaux, A. Garreau and B.E. Benkelfat, "Ultrafast InGaAs/InGaAlAs multiple-quantum-well electro-absorption modulator for wavelength conversion at high bit rates," *Appl. Phys. Lett.*, Vol. 84, pp. 4268-4270, 2004.

[7] A. M. Fox, D. A. B. Miller, G Livescu, J. E. Cunningham and W. Y. Jan, "Quantum well carrier sweep out: relation to electroabsorption and exciton saturation," *IEEE J. Quantum Electron.*, Vol. 27, no. 10, pp. 2281-2295, 1991.

[8] K. S. Abedin, G.-W. Lu, T. Miyazaki, R. Akimoto, and H. Ishikawa, "High-speed all-optical modulation using an InGaAs/AlAsSb quantum well waveguide," *Opt. Express*, vol. 16, no. 13, p. 9684, 2008.

[9] T. Mozume and N. Georgiev, "Optical and structural characterization of InGaAs/AlAsSb quantum wells grown by molecular beam epitaxy," *Japanese J. Appl. Physics, Part 1 Regul. Pap. Short Notes Rev. Pap.*, vol. 41, no. 2 B, pp. 1008–1011, 2002.

[10] R. Akimoto *et al.*, "All-optical demultiplexing of 160-10 Gbits signals with Mach-Zehnder interferometric switch utilizing intersubband transition in InGaAs/AlAs/AlAsSb quantum well," *Appl. Phys. Lett.*, vol. 91, no. 22, pp. 1–4, 2007.

[11] T. Simoyama, S. Sekiguchi, H. Yoshida, J. I. Kasai, T. Mozume, and H. Ishikawa, "Absorption dynamics in all-optical switch based on intersubband transition in InGaAs-AlAs-AlAsSb coupled quantum wells," *IEEE Photonics Technol. Lett.*, vol. 19, no. 8, pp. 604–606, 2007.

[12] A. Neogi, H. Yoshida, T. Mozume, N. Georgiev, and O. Wada, "Intersubband transitions and ultrafast all-optical modulation using multiple InGaAs-AlAsSb-InP coupled double-quantum-well structures," *IEEE J. Sel. Top. Quantum Electron.*, vol. 7, no. 4, pp. 710–717, 2001.

[13] A. Sa'ar and R. Kapon, "Quantum interference, stark, and carrier density infrared electrooptical modulation based on intersubband transitions in asymmetrical quantum wells," *IEEE J. Quantum Electron.*, vol. 33, no. 9, pp. 1517–1526, 1997.

[14] P. Janes and P. Holmstrom, "High-speed optical modulator based on intersubband transitions in InGaAs/InAlAs/AlAsSb coupled quantum wells," *IEEE*, pp. 308–311, 2003.

[15] E. Gross *et al.*, "Measuring the refractive index around intersubband transition resonance in GaN/AlN multi quantum wells," *Opt. Express*, vol. 21, no. 3, p. 3800, 2013.

[16] A. V. Gopal, H. Yoshida, T. Simoyama, N. Georgiev, T. Mozume, and H. Ishikawa, "Well-width and doping-density dependence of 1.35 μm intersubband transition in InGaAs/AlAsSb quantum wells," *Appl. Phys. Lett.*, vol. 80, no. 25, pp. 4696–4698, 2002.

[17] Y. Li, A. Bhattacharyya, C. Thomidis, Y. Liao, T. D. Moustakas, and R. Paiella, "Refractive-index nonlinearities of intersubband transitions in GaN/AlN quantum-well waveguides," *J. Appl. Phys.*, vol. 104, no. 8, pp. 1–6, 2008.

[18] J. Radovanović, V. Milanović, Z. Ikonić, and D. Indjin, "Quantum-well shape optimization for intersubband-related electro-optic modulation properties," *Phys. Rev. B - Condens. Matter Mater. Phys.*, vol. 59, no. 8, pp. 5637–5642, 1999.

[19] H. Yoshida, "Ultrafast all-optical switching and demultiplexing using intersubband transitions in InGaAs/AlAsSb quantum well structures," *Photonics Technol. 21st Century*, vol. 4598, no. 1, pp. 164–174, 2001.

[20] H. Yoshida, T. Mozume, A. Neogi, and O. Wada, "Ultrafast all-optical switching at 1.3 µm/ 1.55 µm using novel InGaAs/AlAsSb/InP coupled double quantum well structure for intersubband transitions," *Electron. Lett.*, vol. 35, no. 13, pp. 40–41, 1999.

[21] F. H. Julien *et al.*, "Nitride intersubband devices: Prospects and recent developments," *Phys. Status Solidi Appl. Mater. Sci.*, vol. 204, no. 6, pp. 1987–1995, 2007.

[22] A. Lupu, M. Tchernycheva, Y. Kotsar, E. Monroy, and F. H. Julien, "Electroabsorption and refractive index modulation induced by intersubband transitions in GaN/AlN multiple quantum wells," *Opt. Express*, vol. 20, no. 11, p. 12541, 2012.

[23] A. Neogi, T. Mozume, H. Yoshida, and O. Wada, "Intersubband transitions at 1.3 and 1.55 µm in a novel coupled InGaAs-AlAsSb double-quantum-well structure," *IEEE Photonics Technol. Lett.*, vol. 11, no. 6, pp. 632–634, 1999.

[24] N. Georgiev and T. Mozume, "Optical properties of InGaAs/AlAsSb type I single quantum wells lattice matched to InP," *J. Vac. Sci. Technol. B Microelectron. Nanom. Struct.*, vol. 19, no. 5, pp. 1747–1751, 2001.

[25] T. Mozume and S. Gozu, "Molecular beam epitaxy and characterization of InGaAs∕AlAs∕AlAsSb coupled double quantum wells with extremely thin coupling barriers," *J. Vac. Sci. Technol. B, Nanotechnol. Microelectron. Mater. Process. Meas. Phenom.*, vol. 28, no. 3, p. C3C25-C3C28, 2010.

[26] T. Mozume, J. I. Kasai, N. Georgiev, T. Simoyama, A. V. Gopal, and H. Yoshida, "Ultralow intersubband absorption saturation intensity at communication wavelength achieved in novel strain compensated InGaAs/AlAs/AlAsSb quantum wells grown by molecular beam epitaxy," *Japanese J. Appl. Physics, Part 1 Regul. Pap. Short Notes Rev. Pap.*, vol. 42, no. 9 A, pp. 5500–5507, 2003.

[27] E. Ozturk and I. Sokmen, "Intersubband optical absorption coefficients and refractive index changes in triple quantum well with different well shapes," *EPJ Appl. Phys.*, vol. 51, pp. 10303-p1-10303-p7, 2010.

[28] A. Neogi, H. Yoshida, T. Mozume, N. Georgiev, T. Akiyama and O. Wada, "Intersubband transition in InGaAs/AlAsSb/ InP in coupled double quantum well structures optimised for communication wavelength operation," *Electron. Lett.*, vol. 36, no. 23, pp. 40–41, 2000.

[29] A. Neogi, H. Yoshida, T. Mozume, N. Georgiev, and O. Wada, "Temperature-insensitive intersubband-transitions in InGaAs/AlAsSb multiple quantum well designed for optical communication wavelength," *Japanese J. Appl. Physics, Part 2 Lett.*, vol. 40, no. 6 A, pp. 38–41, 2001.

[30] H. Ishikawa *et al.*, "Ultrafast all-optical refractive index modulation in intersubband transition switch using InGaAs/AlAs/AlAsSb quantum well," *Japanese J. Appl. Physics, Part 2 Lett.*, vol. 46, no. 8–11, 2007.

[31] J. Zhang, N. Frateschi, R. Jambunathan, W. Choi, and A. E. Bond, "Photonics integrations enabling high-end applications of InP in optical data transmissions," *Optoelectron. Devices Physics, Fabr. Appl. II*, vol. 6013, no. Lim, p. 60130H, 2005.

[32] Y. FEDORYSHYN "Modeling, growth and characterization of InGaAs/AlAsSb quantum well structures for all-optical switching based on intersubband transitions" Ph.D. dissertation, Department of Electronic and Electrical Engineering, ETH ZURICH, 2012.

[33] K.M Wong "Modelling of Intersubband Absorption in Modulation Doped Deep Quantum Wells" Ph.D. dissertation, Department of Electronic and Electrical Engineering, University of Bath, 2007.

[34] M. Trajkovic, ″High speed electro-absorption modulators in indium phosphide generic integration″ Ph.D. dissertation, Department of Electronic and Electrical Engineering, Eindhoven University of Technology, 2019.

[35] N. Kheirodin *et al.*, "Electro-optical intersubband modulators at telecommunication wavelengths based on GaN/AIN quantum wells," *Phys. Status Solidi Appl. Mater. Sci.*, vol. 205, no. 5, pp. 1093–1095, 2008.

[36] Lars Thylén, Urban Westergren, Petter Holmström, Richard Schatz, Peter Jänes, 7-Recent developments in high-speed optical modulators. Royal Institute of Technology (KTH), Kista, Sweden, 2008, pp. 214–215.

Pouyan Matin received the B.Eng. degree in electrical and electronics engineering from the University of Westminster, London, U.K., in 2011 and the M.Sc. degree in telecommunications and computer networks engineering from the London South Bank University (LSBU), London, U.K., in 2013. Since 2017, he has been working toward the Ph.D. degree in nano-photonics engineering at the Photonics Group in the Department of Electronic and Electrical Engineering, University College London (UCL), London, U.K. His research field focuses on electro-absorption modulator design based on semiconductor quantum wells and semiconductor quantum dots, quantum electronics, optoelectronics and nano-photonics.
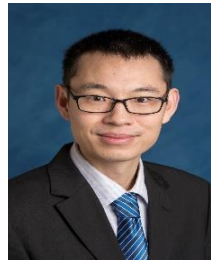
Jiang Wu received the B.S. degree from the University of Electronic Science and Technology of China, Sichuan Sheng, China. He obtained the M.Sc. and Ph.D. degrees in electrical engineering from the University of Arkansas, Fayetteville, AR, USA, in 2008 and 2011, respectively. In 2012, he joined the Photonics Group at University College London (UCL), London, U.K as a Research Associate on molecular beam epitaxy of III-V compound semiconductors and optoelectronic devices. From 2015, he was appointed as Lecturer in the Department of Electronic and Electrical Engineering at UCL. In 2018, He joined Institute of Fundamental and Frontier Sciences (IFFS) at University of Electronic Science and Technology of China (UESTC), Chengdu, Sichuan, China, where he is currently a Professor of semiconductor photonics. His research interests include optoelectronic devices and technologies, Photonics Semiconductor science and information devices, Information function material. He has co-authored more than 100 papers in the area of semiconductor materials and devices.

Huiyun Liu received the Ph.D. degree in semiconductor science from the Institute of Semiconductors, Chinese Academy of Sciences, Beijing, China. In August 2001, he joined the EPSRC National Centre for III-V Technologies, University of Sheffield. He was responsible for the development of molecular beam epitaxy growth of semiconductor materials for the U.K. academic and industrial research community. In 2007, he was awarded Royal Society University Research Fellow and started his academic career in the Department of Electronic and Electrical Engineering, University College London, where he is currently a Professor of semiconductor photonics. His research interests include the nanometer-scale engineering of low-dimensional semiconductor structures (such as quantum dots, quantum wires, and quantum wells) by using molecular beam epitaxy and the development of novel optoelectronic devices including lasers, detectors, and modulators by developing novel device process techniques. He has co-authored more than 300 papers in the area of semiconductor materials and devices.

James Seddon received the B.Sc. degree Chemistry from the University of Plymouth, Plymouth, Devon, U.K., in 2012 and the M.Sc. degree in Nanoscience and Technology from the University of Sheffield, Sheffield, U.K., in 2013. He obtained the M.Res degree in Integrated Photonic and Electronic Systems and the Ph.D. degree in electronics engineering in Ultra-fast Photonics Group at the University College London (UCL), London, U.K. in 2015 and 2019, respectively. He is now a Research Associate and a member of the Photonics Group in the Department of Electronic and Electrical Engineering at UCL working on the development of ultra-high-resolution Terahertz spectrometers. His research interests are Terahertz Spectroscopy and optoelectronics.

Alwyn Seeds received the B.Sc., Ph.D., and D.Sc. degrees from the University of London, London, U.K. From 1980 to 1983, he was a Staff Member at Lincoln Laboratory, Massachusetts Institute of Technology, where he worked on GaAs monolithic millimeterwave integrated circuits for use in phased-array radar. Following three years as a Lecturer in telecommunications at Queen Mary College, University of London, he moved to University College London in 1986, where he is now Professor of opto-electronics and the Head of the Photonics Group. He has published more than 400 papers on microwave and optoelectronic devices and their systems applications. His current research interests include semiconductor optoelectronic devices, wireless and optical communication systems. Prof. Seeds has been a Member of the Board of Governors and the Vice President for Technical Affairs of the IEEE Photonics Society. He has served on the programme committees for many international conferences. He is the Co-founder of Zinwave, a manufacturer of wireless over fibre systems. He was awarded the Gabor Medal and Prize of the Institute of Physics in 2012 and the Distinguished Microwave Educator Award of the IEEE Microwave Theory and Techniques Society in 2018. He is a Fellow of the Royal Academy of Engineering.